Received: 19 May 2022 | Revised: 17 July 2022 | Accepted: 12 August 2022

DOI: 10.1002/ces2.10159

International Journal of Ceramic Engineering & Science

RESEARCH ARTICLE

Photoactivity of nanostructured porous Nb_2O_5: Effect of Pt, Ta, Cu, and Ti impregnation

Leonardo Marasca Antonini[1] | **Janice Adamski**[1] | **Fabiano Bernardi**[2] | **Cesar Aguzzoli**[3] | **Roberto Hübler**[4] | **Célia de Fraga Malfatti**[1]

[1]Corrosion Research Laboratory (LAPEC) – Mining Engineering, Metallurgy and Materials Postgraduate Program (PPGE3M), Federal University of Rio Grande do Sul (UFRGS), Porto Alegre, Rio Grande do Sul, Brazil

[2]Institute of Physics, Federal University of Rio Grande do Sul (UFRGS), Porto Alegre, Rio Grande do Sul, Brazil

[3]Materials Science Graduate Program (PGMAT), University of Caxias do Sul (UCS), Caxias do Sul, Rio Grande do Sul, Brazil

[4]Surface Properties and Interface Study Group (GEPSI) School of Sciences/Pontifical Catholic University of Rio Grande do Sul, TECNOPUC, Porto Alegre, Rio Grande do Sul, Brazil

Correspondence
Leonardo Marasca Antonini, Corrosion Research Laboratory (LAPEC) – Mining Engineering, Metallurgy and Materials Postgraduate Program (PPGE3M), Federal University of Rio Grande do Sul (UFRGS), Porto Alegre, RS, Brazil.
Email: leomantonini@gmail.com

Abstract

In the present work, we report the obtaining of nanostructured porous Nb_2O_5 by anodizing process, with Pt, Ta, Cu, or Ti impregnation, and by magnetron sputtering process. The techniques of scanning electron microscopy, X-ray diffraction, and X-ray photoelectron spectroscopy were used to evaluate the morphology, and the composition and crystalline structure of nanoporous Nb_2O_5. The photocatalytic activity was evaluated by electrochemical photocurrent tests under UV light illumination. Nanostructured porous Nb_2O_5 with Pt, Ta, Cu, and Ti impregnation presented bandgap reduction and 10 times higher photocurrent density in the presence of UV light when compared to the not impregnated nanoporous Nb_2O_5.

KEYWORDS

anodizing process, impregnation, nanoporous Nb_2O_5, photocurrent density

1 | INTRODUCTION

The use of clean and renewable energy is explored on the world stage; the depletion of fossil fuels and the pollution they generate are among the reasons that motivate the research. Solar energy is a renewable and abundant source of energy. Among the researches that stand out for the use of solar energy, one of the most promising ones is the production of H_2 through the dissociation of water from a photocatalyst.[1] The hydrogen generated in this process is converted into electricity without generating polluting gases and as a byproduct only water.[2]

In 1972, Fujishima and Honda[3] presented a methodology for producing H_2 from the dissociation of water, the water splitting process, based on a photocatalyst of metallic oxide in a photoelectricity cell and the application of a small power and solar radiation as a source of excitation.

Similarly, the process can carry out using a semiconductor that has the capacity to absorb the solar energy through the electron/hole pair that acted as reducing and oxidizing agents in the production of H_2 and O_2.[4,5] Titanium dioxide (TiO_2) is the semiconductor most studied because of its structural, electronic, and morphological properties. However, other metallic oxides, such as Ta_2O_5, ZnO, ZrO_2, Fe_2O_3, and Nb_2O_5, also present as photocatalysts in the production of H_2.[6]

Studies using Nb_2O_5 have received attention in recent years and arouse the interest of application that calculates the aggregate value to the niobium for Brazil that holds 98.53% of the world reserves.[7,8] The niobium pentoxide (Nb_2O_5) is a semiconductor that has been studied as a catalyst in reactions, such as esterification, hydrolysis, condensation, alkylation, and dehydration, which still presents great absorption in the region of the ultraviolet that, associated with suitable electronic and textures properties, makes it potentially active for photocatalysis.[9] The high specific surface area, controlled morphology, crystalline phase, and high degree of crystallinity are desired properties of a photocatalyst, which, in the case of niobium, can be finely controlled by the synthesis methodologies.[10–12] In addition, Nb_2O_5 and TiO_2 have a sufficient reduction potential value to transfer electrons from its conduction band to molecular oxygen and reduce the rate of recombination of the charges, thus increasing the efficiency of the photocatalytic process.[13]

However, the separation of the catalyst at the end of the catalytic process and its reuse over several cycles is still a challenge for nanostructured materials as they can disperse in solution, although they present the best results, form colloidal suspensions in aqueous medium, and make it difficult to separate them.[14] The immobilization of the semiconductors in substrates in the form of thin films is an alternative of great potential still to be explored, especially in the case of Nb_2O_5.[15] Another challenge concerns the fact that Nb_2O_5 is only active at light in the ultraviolet region of the electromagnetic spectrum, presenting a bandgap of ~3.4 eV, which means that it is only able to absorb photons with energy greater or equal to that value, and this region corresponds to less than 5% of the solar emission spectrum, whereas the rest of the spectrum is of less energetic photons.[16]

To increase photocatalytic efficiency, the doping process has widely been used in semiconductors. Different papers report a modification in TiO_2 properties when is doped with metals or nonmetals. This modification is related to the incorporation of the ions into the structure of TiO_2 by modifying the physical and chemical properties of the material.[17,18,19] Many transition metals, especially noble metals, such as Au, Pt, Pd, Ir, and Ag, are used as effective dopants to increase photocatalytic activity in H_2 production and/or the degradation of industrial organic materials. These added metals increase the absorption of photons of lower energy, because the metallic and nonmetallic ions can modify the energy of the prohibited band increasing the absorption of the light.[20,4] They still serve as cocatalysts that are added on the surface of semiconductor serving as "traps" for photoelectrons. Thus, when migrating to metallic nanoparticles, the photoelectrons are "trapped," reducing the recombination effect of the electron/hole pair.[21]

Wang et al.[22] studied nanoparticles of TiO_2, Ta_2O_5, and Ta-doped TiO_2 nanoparticles and showed that Ta-doped TiO_2 nanoparticles caused a decrease in bandgap energy of the semiconductor, expanded the wavelength response range to visible region and that the photocatalytic activity was improved by increasing the photogenerated electron/hole pairs. Already, Chittaranjan et al.[23] reported that the doping of titanium dioxide with niobium affects its conductivity and that it improves the photocatalytic performance in the water-splitting reactions.

Platinum has been used as a cocatalyst which is considered the most efficient element in the production of hydrogen,[24] but it is a noble metal, of high cost and scarcity.[25] Copper is a low-cost transition metal and has been reported as an alternative to the use of platinum as a cocatalyst[26]; in addition, copper oxide has photocatalytic action in the predominant range of the solar spectrum, the visible region, with bandgap energy of $E_g \cong 1.9–2.2$ eV.[27]

We present, in this work, nanostructured porous Nb_2O_5 obtained by anodizing process aiming the photocatalytic application. The nanoporous niobium oxides are synthesized from commercially pure niobium through the electrochemical anodizing process and are doped by magnetron sputtering with Pt, Ta, Cu, and Ti, characterized as crystalline structure, chemical composition, and photocatalytic activity.

2 | EXPERIMENTAL PROCEDURES

2.1 | Synthesis of nanoporous Nb_2O_5

Nanoporous niobium oxides were prepared by an electrochemical anodization of niobium metal foil (0.9 cm × 2.5 cm) in an electrolyte containing 1.2-wt% NH_4F, 10% H_2O in glycerol. The samples were used as working electrodes, and a platinum plate was used as a counter electrode. The anodization was carried out at 20°C for 90 min by applying a potential of 90 V.[28] Afterward, the samples were impregnated by magnetron sputtering with the metallic targets of platinum, titanium, tantalum, or copper, with a power of 93 W, 250-mA current, 3×10^{-3} mbar work pressure for 20 s.[29] Finally, the

samples were thermally treated under nitrogen atmosphere at 450°C for 60 min.

2.2 | Characterization of nanoporous Nb_2O_5

The morphology of nanoporous niobium oxides was obtained by anodization evaluated by field emission gun scanning electron microscopy using the TESCAN model MIRA3 operating at 20 kV.

The crystal structure was analyzed by X-ray diffraction (XRD) applying a potential of 40 kV with a current of 40 mA in Philips X-Ray Analytical equipment. The X'Pert HighScore software was used for the analysis and interpretation of the results.

The samples were synthesized and analyzed by X-ray photoelectron spectroscopy (XPS) measurements aiming to determine the chemical components present in the samples. The samples were introduced into the analysis chamber at the D04A-SXS beamline endstation[30] at Brazilian Synchrotron Light Source (LNLS). The measurements were performed at the long scan, Nb 3d, O 1s, C 1s, Ta 4f, Cu 2p, Pt 4f, and Ti 2p scan regions. The spectra were collected using an InSb (111) double-crystal monochromator at fixed photon energies of $h\nu = 1900$ and 3000 eV. The hemispherical electron analyzer (PHOIBOS HSA3500 150 R6) was set at a pass energy of 20 eV ($h\nu = 1900$ eV) and 30 eV ($h\nu = 3000$ eV), and the energy step was 0.1 eV, with an acquisition time of 100 ms/point. The base pressure used inside the chamber was around 5.0×10^{-9} mbar. The monochromator photon energy calibration was done at the Si–K edge (1839 eV). An additional calibration of the analyzer's energy was performed using a standard Au foil (Au $4f_{7/2}$ peak at 84.0 eV). It was also considered the C 1s peak value of 284.5 eV as references to verify possible charging effects. The XPS measurements were obtained at a 45° takeoff angle at room temperature. XPS Peak version 4.1 was used to fit the XPS results. All peaks were adjusted using a Shirley-type background and an asymmetric Gaussian–Lorentzian sum function (23% [$h\nu = 1900$ eV] and 15% [$h\nu = 3000$ eV] Lorentzian contribution).

The bandgap measurements were performed by diffuse reflectance with scanning from 190 to 1700 nm using Varian Cary 5000 equipment and were calculated using the Kubelka–Munk function.

The photoelectrocatalytic behavior was evaluated by a photocurrent test using an Autolab PGSTAT302N potentiostat. A three-electrode cell with platinum as the counter electrode and the Hg/HgO, as the reference electrode, were used in a quartz reactor, and KOH 0.1-M solution was used as an electrolyte. The light source was a 300-W Xenon lamp with a filter AM 1.5 (100 mW/cm^2). The polarization curves were obtained in the presence and absence of light by the application of a potential ramp from the open circuit potential up to 1 V with a sweep speed of 5 mV/s. The photocurrent results were obtained by the subtraction of the photocurrent values measured in the light region and the dark region.[31]

3 | RESULTS AND DISCUSSIONS

3.1 | Morphological and chemical characterization

The formation and growth of the nanostructure on the niobium plates are monitored through the current transient graph as shown in Figure 1A, where it is possible to verify a profile similar to that reported in the literature[32] for the formation of nanotubes. In the present work, the nanostructures obtained are considered nanopores because no individualization of the nanotubes is observed. The accentuated increase in current density in the initial minute is related to the dissolution mechanism followed by a decrease and a new increase less accentuated. This behavior can be related to the formation of the nanopores followed by the formation of the oxide layer and consequent increase in resistance to the passage of electrical current on the surface. Assuad et al.[33] related the second increase in current density with the decrease of the surface resistance caused by the increase of the surface porosity due to the formation of the nanotubes and consequent increase of the surface area. Mueller et al.[34] showed that organic molecules from organic electrolytes can adsorb on the metal surface during the anodizing process in niobium, and this phenomenon hinders the passage of electric current, decreasing current density values and modifying the nanometric morphology.

From the niobium oxide layer (Figure 1C), it is possible to perceive a formation of nanopores with a length of around 500 nm and an internal diameter of around 100–200 nm. Morphology of Nb nanopores after anodization similar to that was found in the work of Altomare et al.[35]

After the formation of a cluster on the niobium oxide surface, was realized the heat treatment aimed at obtaining Nb_2O_5. The XRD depicted in Figure 2 shows that comparing the diffractograms of the samples not treated thermally with the thermally treated samples notes the characteristic peaks related to niobium substrate $2\theta = 38.1°$, 55.3°, and 69.3° according to the standards JCPDS 00-002-1108.

The anodized samples without heat treatment presented a layer of amorphous oxide as reported by other studies.[36,37] The XRD results showed that the heat treatment promoted the formation of a crystalline oxide on the anodized structure (Figure 2).

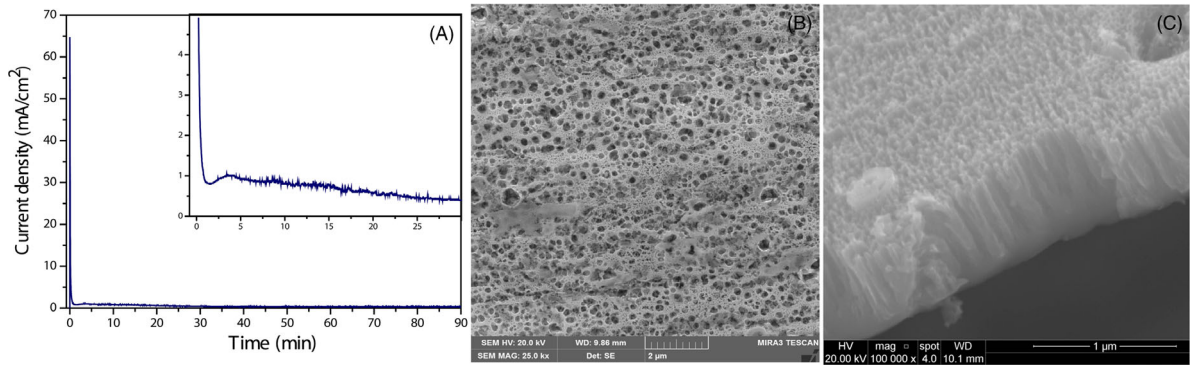

FIGURE 1 Current density transients of the anodized sample and in detail the amplification of the initial region of formation of the nanopores (A); scanning electron microscopy (SEM) images of the surface layer of the anodized Nb (B); and side view of the nanotube layer after anodizing (C)

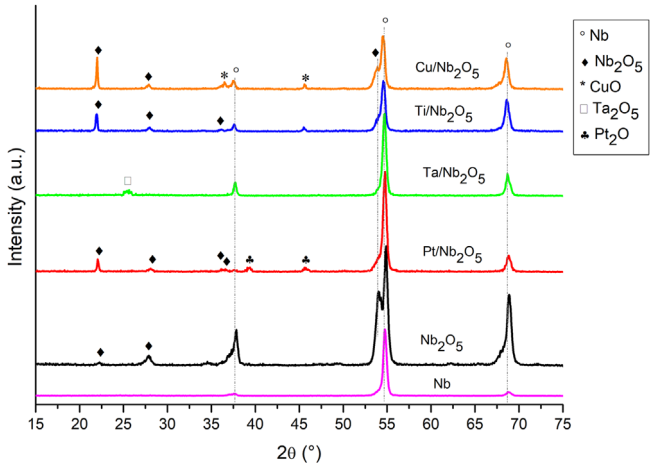

FIGURE 2 X-ray diffraction (XRD) results of anodized samples, impregnated with transition metals and heat treated

The change of the peaks after the heat treatment indicates that a crystalline structure has formed which, according to ICDD (International Center for Diffraction Data), is an orthorhombic structure, compatible with the JCPDS 27-1003 standard. This structure has already been reported by Galstyan et al.,[11] also by Wei et al.,[36] which will report the formation of the orthorhombic crystal structure for nanostructures of Nb_2O_5 after the heat treatment.

In this study, the characteristic peaks of Nb_2O_5 were identified in $2\theta = 27.1°$ assigned to Nb_2O_5 (100) as reported by Galstyan et al.[38] The peaks at $2\theta = 21.5°$ correspond to orthorhombic Nb_2O_5 as indicated by Wei et al.[36] The peaks at $2\theta = 48.8°$ were associated with Nb_2O_5 (110) and the peaks at $2\theta = 54.4°$ with Nb_2O_5 (102).[39,40] According to Liu et al.,[39] the peaks shown in $2\theta = 57.3°$ and $2\theta = 68.4°$ can be associated with Nb_2O_5. Chan et al.[40] performed XRD analyses on heat-treated niobium up to 500°C and found peaks in XRD 27°, 48° and 55° which were identified as Nb_2O_5 of pseudo-hexagonal crystal structure; in addition, these same authors found peaks around 60° and 70° indicated as Nb_2O_5 of a distorted octahedral structure.

In the diffractogram of the Cu-impregnated Nb_2O_5 sample, the characteristic peaks of CuO at $2\theta = 37°$ and 46° were observed, showing that copper was deposited on the surface of the nanopores. From the diffractogram of the Ti-impregnated Nb_2O_5 sample, it was not found characteristic peaks of TiO_2, only peaks associated with Nb_2O_5. In the diffractogram of the Ta-impregnated Nb_2O_5 sample, it is possible to observe, in $2\theta = 25°$, the peak associated with Ta_2O_5.

For the Pt-impregnated Nb_2O_5 sample, two diffraction peaks were observed at $2\theta = 39.8°$ and 46.4°, which were assigned to reflection lines (111) and (200), respectively, of the face-centered cubic structure of Pt_2O (JCPDS 65-5066).

The application of semiconductors for photocatalysis can be optimized by inserting into its crystalline structure atoms of another metal that facilitates the separation of charges inhibiting the electron/hole recombination.[41] The technique of deposition via sputtering allows the formation of clusters of nanostructures with nanometric particles capable of influencing the electron/hole recombination without building up the nanopores. For Ishikawa,[42] the crystalline structure promotes a smooth electron flow from the outside to the inside of the array through the boundaries of the nanocrystals, accompanied by outside-hole consumption and noble metal deposition in the recesses of the surface pores. The crystalline structure contributes to a smooth conduction passage of excited electrons formed by UV irradiation, and pores deposited Pd particles showed good durability and catalytic activity during its use.

In Figure 3, it is possible to observe the micrographies of the surfaces impregnated under 20-s deposition of platinum, tantalum, titanium, or copper, which evidenced that the impregnated surface has not changed. However, from EDS analysis, the presence of the

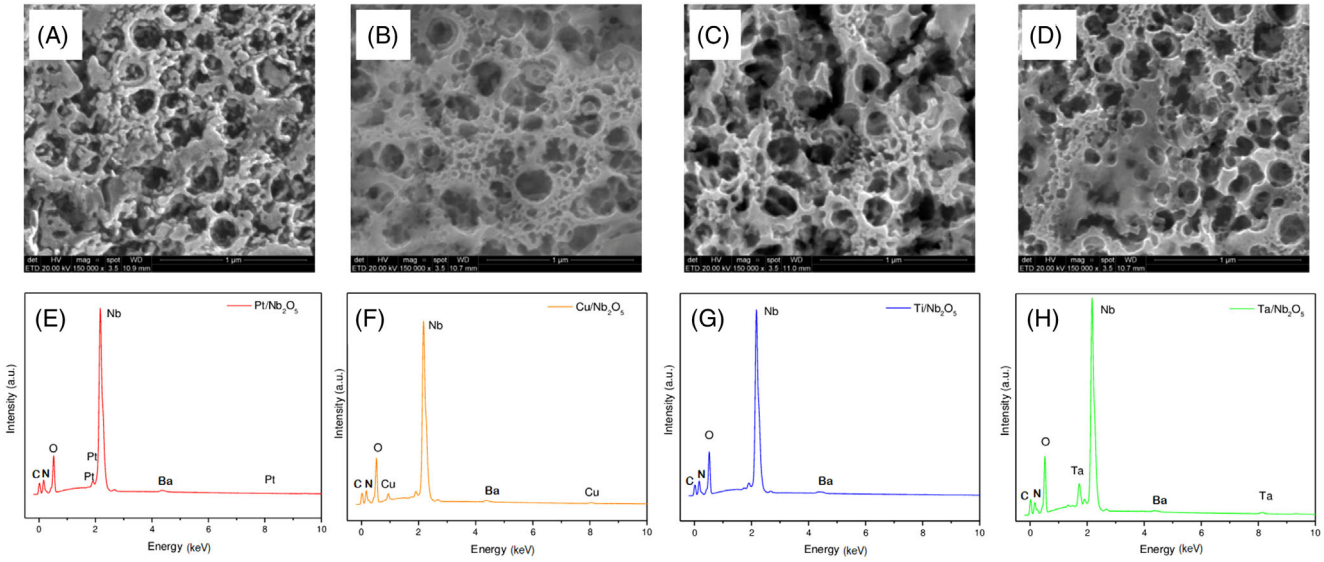

FIGURE 3 Scanning electron microscopy (SEM) images of Nb_2O_5 nanoporous after sputtering deposition of platinum (A), copper (B), titanium (C), and tantalum (D). EDS diffractograms indicative of the presence of the deposited metals: platinum (E), copper (F), titanium (G), and tantalum (H)

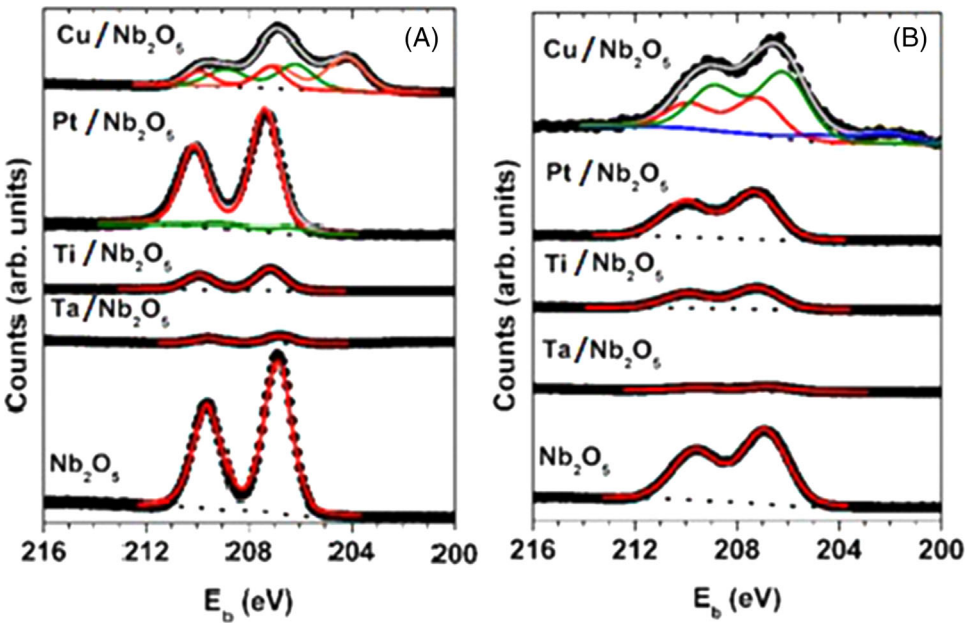

FIGURE 4 Nb 3d X-ray photoelectron spectroscopy (XPS) measurements of the samples impregnated with Cu, Pt, Ti, Ta, and without the formation of cluster measured with (A) $h\nu = 1900$ eV and (B) $h\nu = 3000$ eV. The black points correspond to the experimental data, the dot line the Shirley background, the gray line the best fitting performed, the red line the Nb_2O_5, the green line the NbO_2, the orange line the NbO, and the blue line the metallic Nb component

deposited metal was identified on the surface, as shown in Figure 3.

Figure 4 shows a comparison between the Nb 3d XPS spectra of the samples impregnated for two distinct photon energies of (a) $h\nu = 1900$ eV and (b) $h\nu = 3000$ eV. The change of the photon energy gives a change of the inelastic mean free path from $\lambda = 2.8$ nm ($h\nu = 1900$ eV) to 4.2 nm ($h\nu = 3000$ eV)[43] for the photoelectrons coming from the Nb 3d electronic level. It is possible to observe a clear component associated with Nb_2O_5 for all the samples analyzed. However, the sample impregnated with Pt presents a small component associated with NbO_2 at $h\nu = 1900$ eV. This sample is composed by 93% Nb_2O_5 + 7% NbO_2 in the region probed by this photon energy. At $h\nu = 3000$ eV, the

composition turns to 100% Nb_2O_5, demonstrating the presence of NbO_2 only at the surface of the sample. Moreover, the sample impregnated with Cu shows a huge difference to the other samples concerning the chemical components present at the Nb 3d electronic level. This region is composed by a mixture of 22% Nb_2O_5 + 33% NbO_2 + 45% NbO. The increase of the depth probed in this sample gives a new component associated with metallic Nb. In this case, the chemical components appear as 31% Nb_2O_5 + 59% NbO_2 + 10% NbO. It shows an increase of the presence of metallic Nb with the increase of the depth probed. This result is in accordance with the XRD measurements that probes the bulk region of the sample. Besides that, there is also a shift in the binding energy values of the Nb_2O_5 components, depending on the atom used for decoration. A shift to high values of the modulus of the binding energy can be interpreted as a charge transfer effect from the Nb to surrounding atoms, like those used for decoration, for example.

The spectra with high-energy shifts correspond to the samples with small bandgap values. The sample of Nb anodized, Nb_2O_5 before and Nb_2O_5 after photoreaction presented only the Nb_2O_5 chemical component. The Nb_2O_5 component in the Nb-anodized samples comes from the air exposition because the XPS technique probes the surface region of the sample, in opposition to the XRD measurements that probed the bulk region and a metallic Nb component observed.

Figure 5 shows the XPS spectra at the (A) Ta 4f, (B) Ti 2p, (C) Pt 4f, and (D) Cu 2p electronic regions for both incident photon energies used. The Ta 4f region shows the presence mainly of Ta_2O_5 compound, associated with the Ta^{5+} peak, as expected. However, it also observed a metallic contribution that slightly increases from 3% to 6% when increasing the probed depth. Only the TiO_2 component was observed at the Ti 2p region for both photon energies, associated with the Ti^{4+} 2p3/2 peak. Pt atoms are present as metallic Pt and Pt–O bonding. It was observed a contribution of 31% Pt–O + 69% Pt at $h\nu = 1900$ eV and of 52% Pt–O + 48% Pt at $h\nu = 3000$ eV. The Pt–O comes from the oxidation due to exposition to the air after deposition. The Cu 2p region presents the Cu–O bonding (88%) and the metallic Cu (12%) component at $h\nu = 1900$ eV. The Cu–O comes also from the exposition to the air after deposition. The increased probed depth shows only 8% of Cu–O and 92% of metallic Cu. It shows clearly that the oxidation for Cu atoms takes place at the surface region.

The chemical composition is evidenced by XPS and the results obtained for the compositions of the oxides are obtained in the tests after the depositions with Cu and Pt with their thermodynamic aspects are summarized in Table 1. By the Gibbs free energy variation ($\Delta G°$), as can be seen in the Ellingham diagram for oxides,[44] it is possible to verify that the values of the variation of the free energy of formation of the oxides of Nb ($\Delta G°$ $NbO_2 = -177$ kcal/gfw, NbO = −175 kcal/gfw and $\Delta G°$ $Nb_2O_5 = -164$ kcal/gfw) are smaller, compared to the free energy variation of CuO formation ($\Delta G°$ CuO = −55 kcal/gfw), thus allowing Nb to act as a CuO reductant. This could explain the presence of metallic Cu for the Cu/Nb_2O_5 system (Table 1). The same is true for the Pt/Nb_2O_5 system referenced in Table 1 where an even higher percentage of metallic Pt ($\Delta G°$ PtO = −15 kcal/gfw).

However, the presence of Ti metal has not been observed for the Ti/Nb_2O_5 systems (Table 1), which can explain, thermodynamically, by the fact that the TiO_2 formation energy ($\Delta G°$ $TiO_2 = -205$ kcal/gfw) is even lower than the free energy values of Nb oxides, thus indicating that, thermodynamically, Nb could not act as a reducer of Ti oxides.[39]

In addition, it was observed that the formation of Nb_2O_5 oxide (Table 1) is generally favored at the temperature of the heat treatment at 450°C. As was previously mentioned, the oxides of Nb exhibit values of Gibbs free energy variation of formation very next each other's ($\Delta G°$ $NbO_2 = -177$ kcal/gfw, $\Delta G°$ NbO = −175 kcal/gfw e $\Delta G°$ $Nb_2O_5 = -164$ kcal/gfw) and even though NbO_2 is the most stable form (due to the lower value of free energy variation), the formation of Nb_2O_5 is favored, possibly due to kinetic factors.

A more specific behavior has been observed for Cu/Nb_2O_5 (Table 1), when analyzed with higher energy (3000 eV), that is, at a greater depth. The presence of a large amount of metallic Cu (92%) and even metallic Nb, in addition to 59% of Nb_2O and 31% of Nb_2O_5, is observed. This result may occur due to the reduction of available oxygen for the formation of oxides, considering that the heat treatment done in the atmosphere of N_2. For the Ta/Nb_2O_5 system (Table 1), the presence of 3%–6% of metal fraction is observed as the values of free formation energy of the oxides of Nb are close to that observed for the formation Ta_2O_5 ($\Delta G°$ $Ta_2O_5 = -178$ kcal/gfw); the presence of this metallic fraction may also be associated with the oxygen supply in the system.

3.2 | Photoelectrochemical characterization

Figure 6 shows the UV–Vis diffuse reflectance spectra for the nanoporous Nb_2O_5 impregnated with Ti, Ta, Pt, and Cu and not impregnated. Doping with transition metals decreases the bandgap and reduces the rate of recombination of photogenerated electron–hole pairs. The reduction in bandgap values after impregnation can be associated with change transfer,[45] reflecting in a higher photocurrent

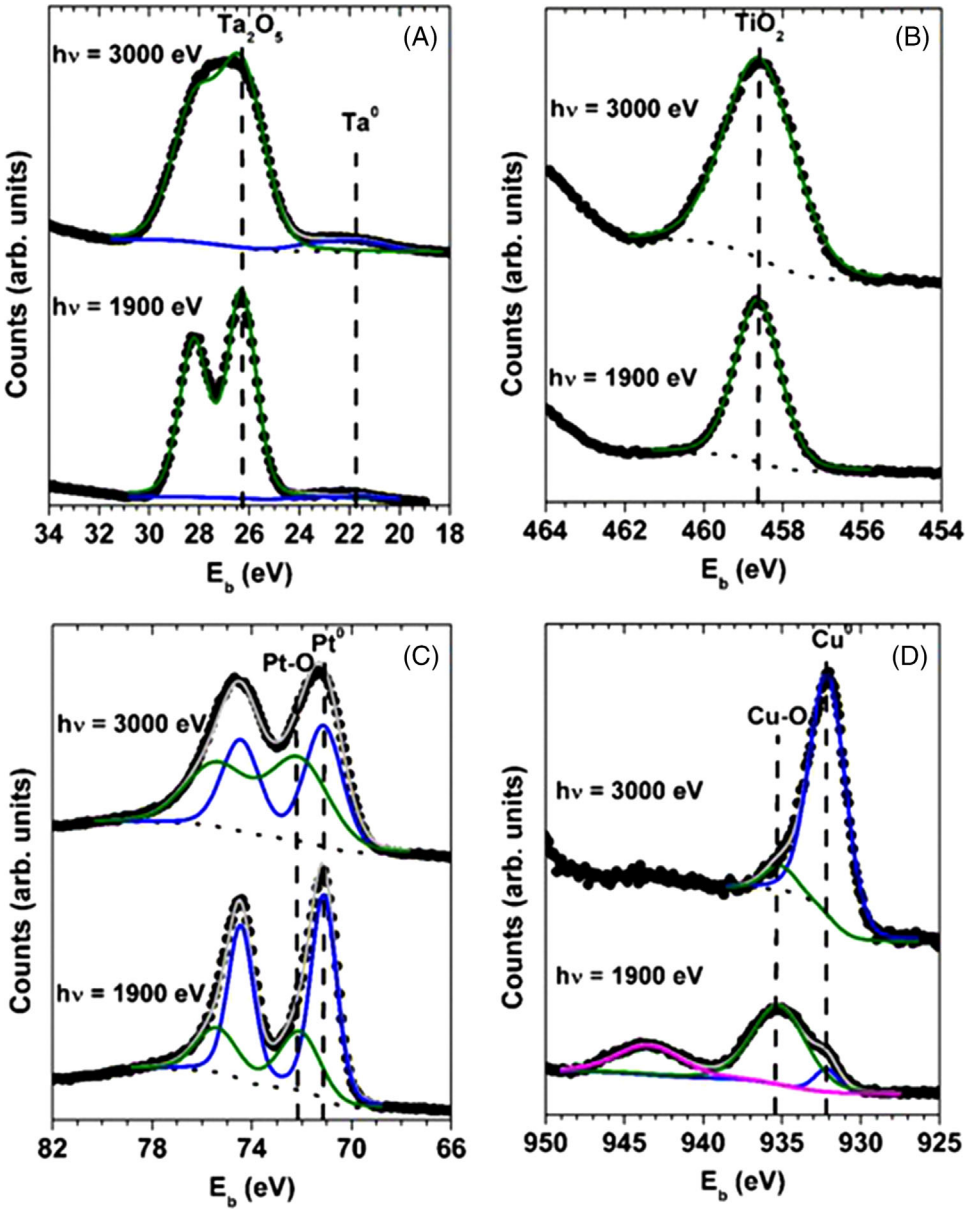

FIGURE 5 X-ray photoelectron spectroscopy (XPS) measurements of the samples impregnated with (A) Ta, (B) Ti, (C) Pt, and (D) Cu atoms at the Ta 4f, Ti 2p, Pt 4f, and Cu 2p electronic regions, respectively. The spectra measured with $h\nu = 1900$ eV or $h\nu = 3000$ eV. The black points correspond to the experimental data, the dot line the Shirley background, and the gray line the best fitting performed. The magenta line represents the satellite contribution.

density (Figure 7). Moreover, photocurrent density values increase from −0.2 V (Figure 7), which causes a more effective charge separation, promoting a better oxidative process.[46]

The presence of the metal deposited can be further evidenced by the alteration of the optical properties. The diffuse reflectance technique demonstrates the alterations of the optical properties of Nb_2O_5 nanoporous impregnated with different metals. The analyzed band showed that all samples prepared are photoactive in the ultraviolet range between 190 and 380 nm as shown in Figure 6.

Applying the Kubelka–Munk equation,[47] the value of the optical bandgap energy is presented in Table 2.

The not impregnated Nb_2O_5 samples had a bandgap value of 3.40 eV; Abe et al. reported bandgap values between 3.4 and 3.1 eV and related this variation to the crystalline structure as the band range of orthorhombic Nb_2O_5 is greater than that of monoclinic Nb_2O_5.[48] For the Nb_2O_5 samples impregnated with TiO_2 presented a bandgap value of 3.32 eV, these results suggest that the formation of clusters of Nb_2O_5 nanoporous with TiO_2 decreases the optic gap of the niobium pentoxide, extending the absorbance in the visible light and, thus,

TABLE 1 Chemical composition at% determined by X-ray photoelectron spectroscopy (XPS)

Sample	Energy (eV)	Nb (%)	NbO (%)	NbO_2 (%)	Nb_2O_5 (%)	Dopant	
						Oxide (%)	Metallic (%)
Nb_2O_5	1900	–	–	–	100	–	–
	3000	–	–	–	100	–	–
Pt/Nb_2O_5	1900	–	–	7	93	31	69
	3000	–	–	–	100	52	48
Cu/Nb_2O_5	1900	–	45	33	22	88	12
	3000	10	–	59	31	8	92
Ta/Nb_2O_5	1900	–	–	–	100	97	3
	3000	–	–	–	100	94	6
Ti/Nb_2O_5	1900	–	–	–	100	100	–
	3000	–	–	–	100	100	–

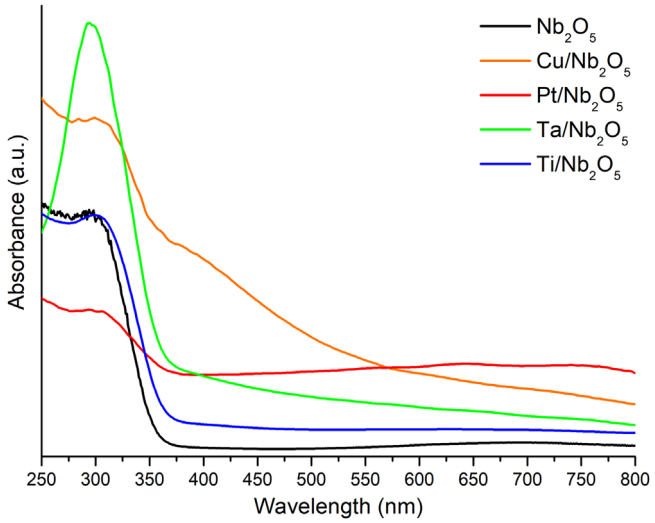

FIGURE 6 UV–Vis diffuse reflectance spectra for the nanoporous Nb_2O_5 impregnated with Ti, Ta, Pt, and Cu and not impregnated

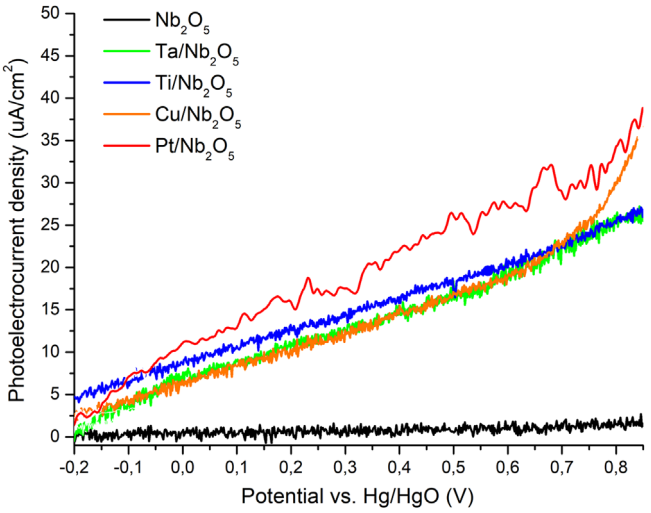

FIGURE 7 Linear scanning voltammogram of the Nb_2O_5 and Nb_2O_5 electrode with Ti, Cu, Ta, or Pt impregnation resulting from the difference between the light region and the dark region. Scanning rate 10 mV/s and electrolyte solution of 0.1-M KOH

TABLE 2 Bandgap values of Nb_2O_5 impregnated nanopores obtained by diffuse reflectance applying the Kubelka–Munk equation

Sample	Bandgap (eV)
Nb_2O_5	3.40
Ti/Nb_2O_5	3.32
Ta/Nb_2O_5	3.29
Pt/Nb_2O_5	2.59
Cu/Nb_2O_5	2.64

increasing the photocatalytic activity.[49] A study realized by Mokhtar et al.[50] showed that the Zr impregnation on Nb_2O_5 nanotubes had a reduction in the bandgap energy from 3.23 to 2.5 eV, which is mainly correlated with the introduced active oxygen vacancies sites within the lattice. The presence of Zr helps one to modify the surface features of Nb_2O_5 and stabilizes the material,[51] enhancing the catalytic behavior of niobium oxide and improving the conductivity and the electron transfer kinetics.[52]

In the samples impregnated with tantalum oxide, the bandgap energy values decreased to 3.29 eV (see Table 2), which clearly demonstrates that the surface nanoporous of Nb_2O_5 is modified by the deposition of the tantalum oxide altering the bandgap. In addition, oxygen vacancies are created when Nb_2O_5 is impregnated with tantalum, which contributes to bandgap narrowing and consequently to increased absorbance in visible light.[53] For Carvalho et al.,[54] the increases of photon absorption, which generate more electron–hole pairs, contribute to increases of photodegradation activity.

The formation of copper clusters resulted in a bandgap value of 2.64 eV; Yoong et al.[55] reported similar result, who

obtained 2.58 eV for the bandgap energy of the copper-doped TiO_2. Thus, in a photocatalytic process, the incident radiation promotes the change of the electrons from the valence band to the conduction band, and the energy of the band is reduced by copper clusters.

With respect to the platinum-impregnated Nb_2O_5 samples, the corresponding bandgap can be calculated at 2.59 eV because of the incorporation of PtO on the surface of the nanoporous. Hu et al.[56] reported a bandgap value of 2.54 eV for TiO_2 doped with platinum indicating that the PtO may be a semiconductor with a hybrid function and stable structure that is capable of being excited by visible light where the electrons could be excited to the conduction band of PtO and then injected into the conduction band of Nb_2O_5 due to the displacement of the conduction band. Influencing the electron–hole recombination process results in high photocatalytic activity.

The voltammogram of Figure 7 shows the increase of the photoactivity for the samples impregnated in ~10 times, which may be related to the capture of holes in the Nb_2O_5 structure, avoiding the recombination of the electrons and making the system more active for photocatalysis. A study carried out by Chwy et al.[57] showed that Nb_2O_5 obtained by anodizing and subsequently impregnated with Li, Na, K, Rb, and Cs showed an increase in photoelectrochemical efficiency when compared to Nb_2O_5 without impregnation. As shown by Esteves et al.,[58] materials with doping metals show a higher percentage of degradation than that obtained with Nb_2O_5 alone; it can be related to materials with lower bandgap, decreasing the energy of the electron/hole pair formation and consequently increasing catalytic activity.

The Nb_2O_5 impregnation with tantalum increases the photoactive performance, as the presence of tantalum increases the vacancies in the Nb_2O_5 acting as active surface sites and increasing the transport of charges. Alim et al.[59] evidenced the increase in photocatalytic performance in TiO_2, and that the photocatalytic properties are deeply influenced by the concentration of titanium vacancies that are the active sites on the surface for the formation of an active complex with water. The concentration of surface-active sites can modify in a controlled manner by the concentration of tantalum incorporated in the semiconductor network and oxygen activity during processing.

The addition of platinum as a cocatalyst in TiO_2 for photocatalysis was reported by Selcuk et al.[60] and Velasquez et al.,[61] and both reported the favoring of photocatalytic activity and increased H_2 production due to its action as an electron or hole remover. On the other hand, there is no strong chemical bond between the particles of the cocatalyst and the nanocrystals of the semiconductor; the Pt particles are adhered to the Nb_2O_5 by metal–support interaction due to the overlapping of the occupied Pt orbitals and orbitals d unoccupied of the Nb_2O_5.

Wang et al.[62] studied the photocatalytic activity of thin films of TiO_2 doped with Cu and obtained a fourfold improvement in the activity of the photocatalyst after doping for methylene blue degradation. The addition of CuO as a cocatalyst is responsible for capturing the photogenerated charge carriers to accelerate the separation of the carriers, which is also because the Fermi level of CuO is lower than that of TiO_2, the transition of the carrier's separation is faster. For Faria et al.,[63] the deposition or impregnation of a small Cu nanoparticles over niobium oxide (Nb_2O_5) increases its photocatalytic activity; this improvement can be attributed to a reduction on the recombination rate of the electron–hole pairs photogenerated due to the electron trapping by Cu species. A study developed by Kanjwal et al.[64] showed that incorporating of silver particles in titanium oxide nanofibers improved the photocatalytic activity of oxide. This behavior can be associated with Ag nanoparticles on titanium oxide surface acting as electron acceptors, enhancing the charge separation of electrons and holes and consequently the transfer of the trapped electron to the adsorbed O_2 acting as an electron acceptor.

4 | CONCLUSIONS

The formation of clusters on the samples by the method of deposition via magnetron sputtering allowed the modification of the surface composition without modifying the nanoporous morphology obtained in the anodization, and it caused the bandgap reduction of the Nb_2O_5 impregnated.

The photocatalysis tests performed with the Nb_2O_5 electrodes impregnated with titanium, tantalum, copper, and platinum showed 10 times higher photocurrent density in the presence of UV light when compared with the not impregnated Nb_2O_5 electrodes.

ACKNOWLEDGMENTS

The present work was developed with the support of the Brazilian government through the National Council for Scientific and Technological Development (CNPq) and CAPES (Brazilian Coordination for the Improvement of Higher Education Personnel), CAPES/UDELAR (047/2013), (CAPES—PROEX Process 23038.000341/2019-71), CNPq (Grant no. 408366/2018-4), and FAPERGS (Grant nos. 19/2551-0002280-8 and 19/2551-0000699-3). Célia de Fraga Malfatti acknowledges CNPq (Grant no. 307723/ 2018-6). L. M. Antonini thanks for the postdoctorate scholarship CAPES PNPD (Grant no. PNPD20132547). We thank the Brazilian Metallurgy and Mining Company (CBMM), by supply the niobium samples, the LCMIC-UCS

and to the Brazilian Synchrotron Light Laboratory (LNLS) for enabling the analysis of XPS.

CONFLICT OF INTEREST

The authors indicated no potential conflicts of interest.

FUNDING INFORMATION

This research did not receive any specific grant from funding agencies in the public, commercial, or not-for-profit sectors.

DECLARATION

All authors certify that they have no affiliations with or involvement in any organization or entity with any financial interest or nonfinancial interest in the subject matter or materials discussed in this manuscript.

ORCID

Leonardo Marasca Antonini https://orcid.org/0000-0002-4961-3436
Célia de Fraga Malfatti https://orcid.org/0000-0002-0819-479X

REFERENCES

1. Armor JN. The multiple roles for catalysis in the production of H_2. Appl Catal A. 1999;176:159–76. https://doi.org/10.1016/S0926-860X(98)00244-0
2. Cook B. An Introduction to fuel cells and hydrogen technology. Vancouver, BC, Canada: Heliocentris; 2001.
3. Fujishima A, Honda K. Electrochemical photolysis of water at a semiconductor electrode. Nature. 1972;238:37–8. https://doi.org/10.1038/238037a0
4. Paramasivam I, Jha H, Liu N, Schmuki P. A review of photocatalysis using self-organized TiO_2 nanotubes and other ordered oxide nanostructures. Small. 2012;8:3073–103. https://doi.org/10.1002/smll.201200564
5. Zhou C, Shi R, Waterhouse GIN, Zhang T. Recent advances in niobium-based semiconductors for solar hydrogen production. Coord Chem Rev. 2020;419:213399. https://doi.org/10.1016/j.ccr.2020.213399
6. Chen X, Shen S, Guo L, Mao S. Semiconductor-based Photocatalytic hydrogen generation. Chem Rev. 2010;110:6503–70. https://pubs.acs.org/doi/10.1021/cr1001645
7. Alves RA, Coutinho AR. The evolution of the niobium production in Brazil. Mater Res (São Carlos, Brazil). 2015;18:106–12. http://doi.org/10.1590/1516-1439.276414
8. Horst JD. Perspectives over the Brazilian iron-niobium production. Open Access J Sci. 2018;2:67–8. http://doi.org/10.15406/oajs.2018.02.00046
9. Prado AGS, Bolzon LB, Pedroso CP, Moura AO, Costa L. Nb_2O_5 as efficient and recyclable photocatalyst for indigo carmine degradation. Appl Catal B. 2008;82:219–24. https://doi.org/10.1016/j.apcatb.2008.01.024
10. Liu X, Yuan R, Liu Y, Zhu S, Lin J, Xianfeng X. Niobium pentoxide nanotube power for efficient dye-sensitized solar cells. New J Chem. 2016;40:6276–80. https://doi.org/10.1039/C6NJ00159A
11. Galstyan V, Comini E, Faglia G, Sberveglieri G. Synthesis of self-ordered and well-aligned Nb_2O_5 nanotubes. CrystEngComm. 2014;16:10273–9. https://doi.org/10.1039/C4CE01540A
12. Pei L, Yang M, Zhang D, Chen P, Song Y, Gan Y. Photoelectrochemical activities and low content Nb-doping effects on one-dimensional self-ordered Nb_2O_5-TiO_2 nanotubes. RSC Adv. 2015;5:9138–42. https://doi.org/10.1039/C4RA12180E
13. Mourão HAJL, Avansi W Jr, Ribeiro C. Hydrothermal synthesis of Ti oxide nanostructures and TiO_2:SnO_2 heterostructures applied to the photodegradation of rhodamine B. Mater Chem Phys. 2012;135:524. https://doi.org/10.1016/j.matchemphys.2012.05.019
14. Mourão HAJL, Malagutti AR, Ribeiro C. Synthesis of TiO_2-coated $CoFe_2O_4$ photocatalysts applied to the photodegradation of atrazine and rhodamine B in water. Appl Catal A. 2010;382:284–92. https://doi.org/10.1016/j.apcata.2010.05.007
15. Costa RGF, Oliveira JE, Paula GF, Picciani PHS, Medeiros ES, Ribeiro C, et al. Electrospinning of polymers in solution. Part I: Theoretical foundation. Polímeros. 2012;22:170–7. http://doi.org/10.1590/S0104-14282012005000026
16. Chen Q, Liu H, Xin Y, Cheng X, Zhang J, Li J, et al. Controlled anodic growth of TiO_2 nanobelts and assessment of photoelectrochemical and photocatalytic properties. Electrochim Acta. 2013;99:152–60. https://doi.org/10.1016/j.electacta.2013.03.032
17. Preethi LK, Antony RP, Mathews T, Loo SCJ, Wong LH, Dash S, et al. Nitrogen doped anatase-rutile heterostructured nanotubes for enhanced photocatalytic hydrogen production: promising structure for sustainable fuel production. Int J Hydrogen Energy. 2016;41:5865–77. https://doi.org/10.1016/j.ijhydene.2016.02.125
18. Zhao Z, Sun J, Xing S, Liu D, Zhang G, Bai L, et al. Enhanced Raman scattering and photocatalytic activity of TiO_2 films with embedded Ag nanoparticles deposited by magnetron sputtering. J Alloys Compd. 2016;679:88–93. https://doi.org/10.1016/j.jallcom.2016.03.248
19. Fan X, Wan J, Liu E, Sun L, Hu Y, Li H, et al. High-efficiency photoelectrocatalytic hydrogen generation enabled by Ag deposited and Ce doped TiO_2 nanotube arrays. Ceram Int. 2015;41:5107–16. https://doi.org/10.1016/j.ceramint.2014.12.083
20. Lin X, Rong F, Ji X, Fu D, Yuan C. Preparation, and enhanced visible light photocatalytic activity of N-doped titanate nanotubes by loaded with Ag for degradation of X-3B. Solid State Sci. 2011;13:1424–8. https://doi.org/10.1016/j.solidstatesciences.2011.05.005
21. Leung DYC, Fu X, Wang C, Ni M, Leung MKH, Wang X, et al. Hydrogen production over titania-based photocatalysts. ChemSusChem. 2010;3:681–94. https://doi.org/10.1002/cssc.201000014
22. Wang C, Geng A, Guo Y, Jiang S, Qu X. Three-dimensionally ordered macroporous Ti1−xTaxO_2+x/2 (x = 0.025, 0.05, and 0.075) nanoparticles: preparation and enhanced photocatalytic activity. Mater Lett. 2006;60:2711–4. https://doi.org/10.1016/j.matlet.2006.01.109
23. Chittaranjan D, Roy P, Yang M, Jha H, Schmuki P. Nb doped TiO_2 nanotubes for enhanced photoelectrochemical water-splitting. Nanoscale. 2011;3:3094–6. https://doi.org/10.1039/C1NR10539F
24. Teoh WY, Mädler L, Amal R. Inter-relationship between Pt oxidation states and the photocatalytic mineralization of organic

matters. J Catal. 2007;251:271–80. https://doi.org/10.1016/j.jcat.2007.08.008
25. Wang C, Fan H, Ren X, Wen Y, Wang W. Highly dispersed PtO nanodots as efficient co-catalyst for photocatalytic hydrogen evolution. Appl Surf Sci. 2018;462:423–31. https://doi.org/10.1016/j.apsusc.2018.08.126
26. Lucchetti R, Onotri L, Clarizia L, Natale FD, Somma ID, Andreozzi R, et al. Removal of nitrate and simultaneous hydrogen generation through photocatalytic reforming of glycerol over "in situ" prepared zero-valent nano copper/P25. Appl Catal B. 2017;202:539–49. https://doi.org/10.1016/j.apcatb.2016.09.043
27. Wu HW, Lee SY, Lu WC, Chang KS. Piezoresistive effects enhanced the photocatalytic properties of Cu_2O/CuO nanorods. Appl Surf Sci. 2015;344:236–41. https://doi.org/10.1016/j.apsusc.2015.03.122
28. Adamski J, Antonini LM, Iser TV, Ortega MR, Aguzzoli C, Malfatti CF. Photoelectrochemical performance of anodized niobium for hydrogen production. RE&PQJ. 2018;1:242–6. https://doi.org/10.24084/repqj16.273
29. Tentardini EK, Blando E, Hübler R. TiN structural modifications induced by bias voltage in a new dynamic controlled magnetron sputtering apparatus. Nucl Instrum Methods Phys Res Sect B. 2001;175:626–9. https://doi.org/10.1016/S0168-583X(00)00652-2
30. Abbate M, Vicentin FC, Compagnon-Cailhol V, Rocha MC, Tolentino H. The soft X-ray spectroscopy beamline at the LNLS: technical description and commissioning results. J Synchrotron Radiat. 1998;5:539–41. https://doi.org/10.1107/S0909049599008122
31. Palmas S, Polcaro AM, Ruiz JR, Da Pozzo A, Mascia M, Vacca A. TiO2 photoanodes for electrically enhanced water splitting. Int J Hydrogen Energy. 2010;35:6561–70. https://doi.org/10.1016/j.ijhydene.2010.04.039
32. Sieber I, Hildebrand H, Freidrich A, Schmuki P. Formation of self-organized niobium porous oxide on niobium. Electrochem Commun. 2005;7:97–100. https://doi.org/10.1016/j.elecom.2004.11.012
33. Assuad L, Schumacher J, Tafel A, Bochmann S, Christiansen S, Bachmann J. Systematic increase of electrocatalytic turnover at nanoporous platinum surfaces prepared by atomic layer deposition. J Mater Chem A. 2015;3:8450–8. https://doi.org/10.1039/C5TA00205B
34. Mueller LT, Oliveiras KV, Morisson FDP, Kunst SR, Carone CLP, Oliveira CT. Influência da concentração de ácido acético presente no licor pirolenhoso na anodização de nióbio. Technol Metall Mater Min. 2021;18:1–9. https://doi.org/10.4322/2176-1523.20212314
35. Altomare M, Cha G, Schmuki P. Anodic nanoporous niobium oxide layers grown in pure molten ortho-phosphoric acid. Electrochim Acta. 2020;344:136–58. https://doi.org/10.1016/j.electacta.2020.136158
36. Wei W, Lee K, Shaw S, Schmuki P. Anodic formation of high aspect ratio, self-ordered Nb_2O_5 nanotubes. Chem Commun. 2012;48:4244–6. https://doi.org/10.1039/C2CC31007D
37. Sampaio EJP, Antonini LM, Júnior AGS, Andrade AMH, Malfatti CF, Hubler R, et al. Highly ordered nanotubular niobium oxide obtained by self-organizing anodization: A study of capacitive behavior. Ceram Int. 2022;48:25424–30. In Press. https://doi.org/10.1016/j.ceramint.2022.05.219
38. Galstyan V, Comini E, Faglia G, Sberveglieri G. Synthesis of self-ordered and well-aligned Nb_2O_5 nanotubes. CrystEngComm. 2014;16:10273–9.
39. Liu X, Yuan R, Liu Y, Zhu S, Lin J, Chen X. Niobium pentoxide nanotube powder for efficient dye-sensitized solar cells. New J Chem. 2016;40:6276–80.
40. Chan X, Pu T, Chen X, James A, Lee J, Parise JB, et al. Effect of niobium oxide phase on the furfuryl alcohol dehydration. Catal Commun. 2017;97:65–9.
41. Gálvez JB, Rodrigues SM, Gasca CAE, Bandala ER, Gelover S, Leal T. Purificación de águas por fotocatálisis heterogênea: estado Del arte. In: Miguel A, editor. Eliminación de contaminantes por fotocatálisis Heterogénea, Red CYTED VIII-G. La Plata: Blesa; 2001. p. 51–76
42. Ishikawa T. High-performance photocatalyst containing noble metals selectively deposited inside mesopore. Int J Appl Ceram Technol. 2022;19:181–7. https://doi.org/10.1111/ijac.13777
43. Tanuma S, Powell CJ, Penn DR. Calculations of electron inelastic mean free paths II. Data for 27 elements over the 50–2000 eV range. Surf Interface Anal. 1991;17:911–26. https://doi.org/10.1002/sia.740171304
44. Reed TB. Free energy of formation of binary compounds. Cambridge, MA: MIT Press; 1971.
45. Brito JF, Mascaro LH. Enhancement of photocurrent response for self-ordered Nb2O5 nanotubes synthesized at room temperature. J Mater Sci. 2021;56:2088–102. https://doi.org/10.1007/s10853-020-05317-8
46. Bessegato GG, Cardoso JC, Da SBF, Zanoni MVB. Enhanced photoabsorption properties of composites of Ti/TiO_2 nanotubes decorated by Sb2S3 and improvement of degradation of hair dye. J Photochem Photobiol A. 2014;276:96–103. https://doi.org/10.1016/j.jphotochem.2013.12.001
47. Murphy AB. Band-gap determination from diffuse reflectance measurements of semiconductor films, and application to photoelectrochemical water-splitting. Sol Energy Mater Sol Cells. 2007;91:1326–37. https://doi.org/10.1016/j.solmat.2007.05.005
48. Abe S. Formation of Nb_2O_5 matrix and vis-NIR absorption in Nb-Ge-O thin film. Nanoscale Res Lett. 2012;7:1–6. https://doi.org/10.1186/1556-276X-7-341
49. Silva A, Muche DNF, Dey S, Hotza D, Castro RHR. Photocatalytic Nb_2O_5-doped TiO_2 nanoparticles for glazed ceramic tiles. Ceram Int. 2016;42:5113–22. https://doi.org/10.1016/j.ceramint.2015.12.029
50. Mokhtar AM, Salem KE, Allam NK. Multiple synergistic effects of Zr-alloying on the phase stability and photostability of black niobium oxide nanotubes as efficient photoelectrodes for solar hydrogen production. Appl Catal B. 2021;287:119961. https://doi.org/10.1016/j.apcatb.2021.119961
51. Fawzy SM, Omar MM, Allam NK. Photoelectrochemical water splitting by defects in nanostructured multinary transition metal oxides. Sol Energy Mater Sol Cells. 2019;194:184–94. https://doi.org/10.1016/j.solmat.2019.02.011
52. Salem KE, Mokhtar AM, Abdelhafiz A, Allam NK. Niobium–zirconium oxynitride nanotube arrays for photoelectrochemical water splitting. ACS Appl Nano Mater. 2020;3:6078–88. https://doi.org/10.1021/acsanm.0c01282
53. Rengifo-Herrera JA, Pierzchala K, Sienkiewicz A, Forro L, Kiwi J, Pulgarin C. Abatement of organics and *Escherichia coli* by N, S co-doped TiO_2 under UV and visible light. Implications of the

formation of singlet oxygen (1O2) under visible light. Appl Catal B. 2009;88:398–406. https://doi.org/10.1016/j.apcatb.2008.10.025
54. Carvalho GSG, Siqueira MM, Nascimento MP, Oliveira MAL, Amarante GW. Nb_2O_5 supported in mixed oxides catalyzed mineralization process of methylene blue. Heliyon. 2020;6:1–7. https://doi.org/10.1016/j.heliyon.2020.e04128
55. Yoong LS, Chong FK, Dutta BK. Development of copper-doped TiO_2 photocatalyst for hydrogen production under visible light. Energy. 2009;34:1652–61. https://doi.org/10.1016/j.energy.2009.07.024
56. Hu Y, Song X, Jiang S, Wei C. Enhanced photocatalytic activity of Pt-doped TiO_2 for NOx oxidation both under UV and visible light irradiation: a synergistic effect of lattice Pt4+ and surface PtO. Chem Eng J. 2015;274:102–12. https://doi.org/10.1016/j.cej.2015.03.135
57. Chwy T, Ji S, Ye C, Iwase A. In situ metal doping during modified anodization synthesis of Nb_2O_5 with enhanced photoelectrochemical water splitting. AIChE J. 2016;62:352–8. https://doi.org/10.1002/aic.15048
58. Esteves A, Oliveira LCA, Ramalho TC, Gonçalves M, Anastácio AS, Carvalho HWP. New materials based on modified synthetic Nb_2O_5 as photocatalyst for oxidation of organic contaminants. Catal Commun. 2008;10:330–2.
59. Alim MA, Bak T, Atanacio A, Ionescu M, Kennedy B, Price WS, et al. Photocatalytic properties of Ta-doped TiO_2. Ionics. 2017;23:3517–31. https://doi.org/10.1007/s11581-017-2162-2
60. Selcuk H, Zaltner W, Sene JJ, Bekbolet M, Anderson MA. Photocatalytic and photoelectrocatalytic performance of 1% Pt doped TiO_2 for the detoxification of water. J Appl Electrochem. 2004;34:653–8. https://doi.org/10.1023/B:JACH.0000021931.36151.54
61. Velasquez JJ, González RF, Díaz L, Melián EP, Rodríguez VD, Núñez P. Effect of reaction temperature and sacrificial agent on the photocatalytic H_2-production of Pt-TiO_2. J Alloys Compd. 2017;721:405–10. https://doi.org/10.1016/j.jallcom.2017.05.314
62. Wang S, Meng KK, Zhao L, Jiang Q, Lian JS. Superhydrophilic Cu-doped TiO_2 thin film for solar-driven photocatalysis. Ceram Int. 2014;40:5107–10. https://doi.org/10.1016/j.ceramint.2013.09.028
63. Faria AL, Centurion HA, Torres JA, Gonçalves RV, Ribeiro LS, Riberio C, et al. Enhancing Nb_2O_5 activity for CO_2 photoreduction through Cu nanoparticles cocatalyst deposited by DC-magnetron sputtering. J CO2 Util. 2021;53:101739. https://doi.org/10.1016/j.jcou.2021.101739
64. Kanjwal MA, Barakat NAM, Sheikh FA, Khil MS, Kim HY. Functionalization of electrospun titanium oxide nanofibers with silver nanoparticles: strongly effective photocatalyst. Int J Appl Ceram Technol. 2010;7:E54–63. https://doi.org/10.1111/j.1744-7402.2009.02397.x

How to cite this article: Antonini LM, Adamski J, Bernardi F, Aguzzoli C, Hübler R, de Fraga Malfatti C. Photoactivity of nanostructured porous Nb_2O_5: Effect of Pt, Ta, Cu, and Ti impregnation. Int J Ceramic Eng Sci. 2022;4:379–390. https://doi.org/10.1002/ces2.10159